Proceedings of 20th Iranian Conference on Biomedical Engineering (ICBME 2013), University of Tehran, Tehran, Iran,
December 18-20, 2013

A Fully Automated Segmentation of Radius Bone Based on Active Contour in Wrist MRI Data Set

Hamed Yousefi[1] hamed.yousefi@ut.ac.ir
Mansoor Fatehi[2] fatehi@irsr.org
Mehdi Amian[1] mehdi.amian@ut.ac.ir
Reza A. Zoroofi[1] zoroofi@ut.ac.ir

[1] Control and Intelligent Processing Center of Excellence, School of Electrical and Computer Engineering, University of Tehran, Tehran, Iran
[2]Iranian Society of Radiology, Tehran, Iran

***Abstract*— Advanced medical imaging techniques require high performance segmentation algorithms. Extracting the structures of interest accurately is one of the main challenges in medical imaging segmentation. In this paper a methodological approach based on active contour is proposed for fully automated segmentation of radius bone. As soft tissues like tendons, muscles and fat around the bone have close intensities to internal parts of the bone, accurate segmentation is difficult. Here the designed framework takes an MR image including radius bone as input and produces the segmented radius bone in 3D voxel set. The multi-step approach for segmentation is as following. Since our data set was much noisier, at first we denoised and enhanced contrast of the data using wavelet transform. Then an initial segmentation was produced focusing on edge map. Next, according to anatomical knowledge about the radius bone shape and size in intermediate slices, radius bone was extracted in this slice and used as the mask slice for adjacent slices. This masking procedure was applied to all slices with a 3D approach. After that we derived a convex hull region around the radius bone. This step was done for whole slices as regions of interest. Finally the estimated convex region is used as an initial mask for active contour. This framework was tested on more than 600 coronal MR slices of 23 subjects. In comparison to manual segmentation our method showed an average Dice similarity coefficient DSC and kappa statistics of 94.82% and 92.46% respectively. In the future works we utilize the proposed approach as part of a computer-aided diagnosis system for bone age estimation.**

Keywords-coronal slice; wavelet transform; edge map; initial mask.

I. Introduction

Advanced medical imaging techniques require high performance segmentation algorithms. The main challenge in medical image segmentation tasks is to extract accurately the structures of interest. In the case of medical imaging the segmentation process can be taken place in 2D or in the 3D space. 2D algorithms can be extended to 3D medical volumes by being applied successively on the compounding 2D slices. The last approach is in some cases more practical as it is easier to implement, it requires less memory, and has lower computation complexity.

Active contour methods have been widely applied in medical image segmentation tasks [1] [2] [3]. Their ability to adjust contours to the structures with irregular shapes made them suitable for brain segmentation tasks or tumor region detection. They were also used for segmenting 3D volumetric MRI datasets for image guided surgery tasks [4]. Jiang [5] combined the active contours approach with morphological operations for the X-ray bone segmentation in CT datasets.

A. Segmentation of bone structures in MRI

In general, a bone can be divided in two parts: the cancellous bone, the interior part, generally consisting of fat, which is represented by bright areas in MR images and the cortical bone, the exterior calcified section of the bone which can be identified as dark regions in the MR datasets (because of the lack of fat or water protons). Therefore the algorithm focuses on the segmentation of the boundary between high intensity signal inside the cancellous bone and the cortical bone. Around the bones there are other soft tissues, such as tendons, muscles, and fat, with similar intensities to those of the internal parts of the bone, which make the segmentation process very difficult.

This is the reason for which in some cases it is delicate to accurately decide on the boundary of the bone. The aforementioned elements in the human hand are sometimes difficult to clearly identify, because their appearance depends on the MRI characteristics (the parameters of the scanning process).

So, a segmentation algorithm is needed to be developed for the accurate segmentation of bone structures in 3D MRI dataset so that it would be able to overcome the shortcomings of the other present imaging techniques. Some of the challenges in this field are noise, intensity inhomogeneity, and partial volume effects.

B. Noise in MR Imaging

In magnetic resonance imaging (MRI) there is a trade-off between signal-to-noise ratio (SNR), acquisition time and spatial resolution. Another important source of noise in MR imaging is thermal noise of the human body. Common MR imaging involves sampling in the frequency domain (also called "k-space"), and the MRI image is computed using the Inverse Discrete Fourier Transform (IDFT). Signal measurements have components in both real and imaginary channels and each channel is affected by additive white Gaussian noise. Thus, the complex reconstructed signal includes a complex white additive Gaussian noise.

C. *Partial volume effect*

The partial volume effect (PVE) is the consequence of the limited resolution of the scanning hardware and the discretization procedures. It occurs in non-homogeneous areas, where several anatomical entities contribute to the gray-level intensity of a single pixel/voxel. It results in blurred intensities across edges, making difficult the task of accurately deciding on the borders of two connected objects.

Another similar artifact is called fat/water cancelling and emerges in regions containing mutually fat and water. Due to their opposing magnetization fields, the corresponding regions will appear dark.

D. *Inhomogenity shortcomin*

Another difficulty which has to be handled by segmentation techniques using MR images is the intensity inhomogeneity shortcoming. The intensity inhomogeneity's can be caused by the imperfections in the RF coil that produces the magnetic field, or by various harms in the signal acquisition procedures. Also, the magnetic field can have a non-uniform distribution due to the local magnetic properties of the studied biological structure or because of a movement of the patient during the acquisition process. This effect can be identified as shading artifacts in the image data and can have a major consequence on the performances of the intensity based segmentation algorithms, considering that a certain tissue has a constant intensity distribution in the dataset [6].

II. METHODS

A framework was designed that requires a set of 2-D coronal MR images including the wrist hand information as input and provides segmentation of the radius bone in the form of3-D voxel points as output. The individual components of our framework are outlined as follows.

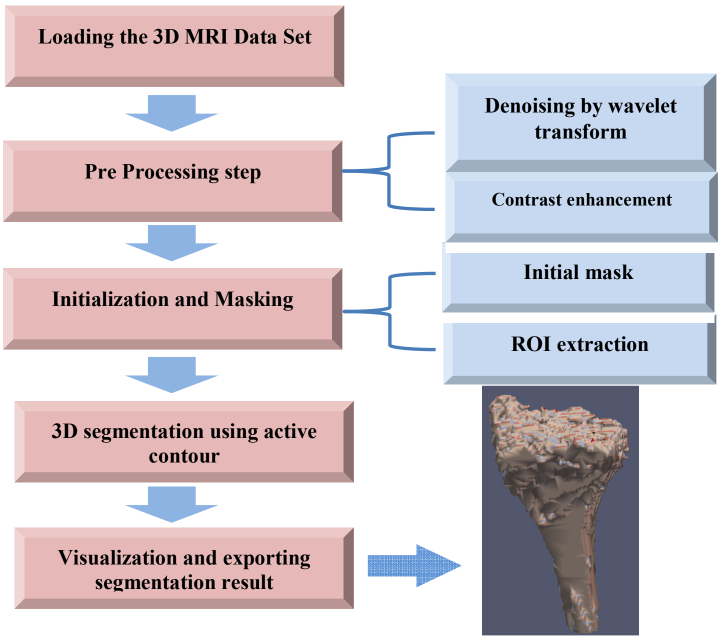

Figure 1. Block diagram of the proposed method

In this method, MR images of 27 coronal slices of hand wrist as the input of the algorithm and the radius bone in the form of 3D voxels as the output. All steps are fully automatic and there is no need to a human or initial point.

Dataset consists of 27 T1-weighted images of hand wrist in coronal view which we are provided by Peyambaran hospital (Abazar street, Tehran, IRAN). It's usual to acquire this kind of images in 9 slices. But this dataset uses 27 slices which results a reduction in depth in 3:1 ratio. Case studies are 23 players of Iran's national youth team whose age is under 17.

A. *Preprocessing*

This section is composed of two parts: noise reduction and image enhancement.

.All digital images contain some degree of noise due to the corruption in its acquisition and transmission by various effects. Particularly, medical image are likely disturbed by a complex type of addition noise depending on the devices which are used to capture or store them. No medical imaging devices are noise free. The most commonly used medical images are received from MRI equipment's. Usually, the addition noise into medical image reduces the visual quality that complicates diagnosis and treatment.

The way the magnitude MRI image is reconstructed results in a Rician distribution of the noise. The main remark is that the Rician noise is signal-dependent, separating the signal from noise being a very difficult task. In high intensity areas of the magnitude image, Rician distribution can be approximated to a Gaussian distribution, and in low intensity regions it can be estimated as a Rayleigh distribution. A practical effect is a reduced contrast of the MRI image, as the noise increases the mean intensity values of the pixels in low intensity regions. As explained, it is a fact that Rician noise degrades the MRI images in both qualitative and quantitative senses, making image processing, interpretation and segmentation more difficult. Consequently, it is important to develop an algorithm to filter this type of noise [7].

Because the wavelet transform has an ability to capture the energy of a signal in few energy. The wavelet denoising techniques offers high quality and flexibility for the noise problem of signals and image.

Also, the sharpening filter was applied to the denoised image in order to enhance the image, make better the separability of bone tissue, and detect the edge.

B. *Initialization and Masking*

In MR images unlike to CT images, because of partial volume effect and additive noise which explained previously, seperability of bone region from other tissues would be done difficultly. So, dynamic threshold method cannot be useful and may lead to misidentification of radius bone in 3D approach of slice masking. Thus, the proposed method was based on edge map focusing.

$$E^{i}_{merge} = E^{i}_{\sigma 2} + E^{i}_{internal\_morph} + E^{i}_{\sigma 3, close\_morph} \qquad (1)$$

$$S^i = F\,(E^i{}_{merge}) - E^i{}_{threshold} \tag{2}$$

As (2) implies the edge map focusing is composed of two phases. First, in (1) $E^i{}_{merge}$ is edge map including integration of Canny operator with a variance as 2, $E^i{}_{\sigma 2}$ and the resulted edge from operator morphology erosion, $E^i{}_{internal\_morph}$ where i is i-th slice. The epiphyseal plate which passes through the radius bone causes disconnectivity in radius bone region. Therefore, we used the map edge $E^i{}_{\sigma 3, close\_morph}$ which consists of Canny edge detector with a variance as 3 and the morphology operator closing with a vertical structure element containing 6 pixels. At last, we accomplish the first phase by using morphology operator filling. In (2), F is the filling morphological operator. Second, the denoised image resulted from dynamic threshold method, is subtracted from the output image of the first phase. Thus, we obtain an approximate image of radius bone that fully separated from other regions and is very important for masking stage.

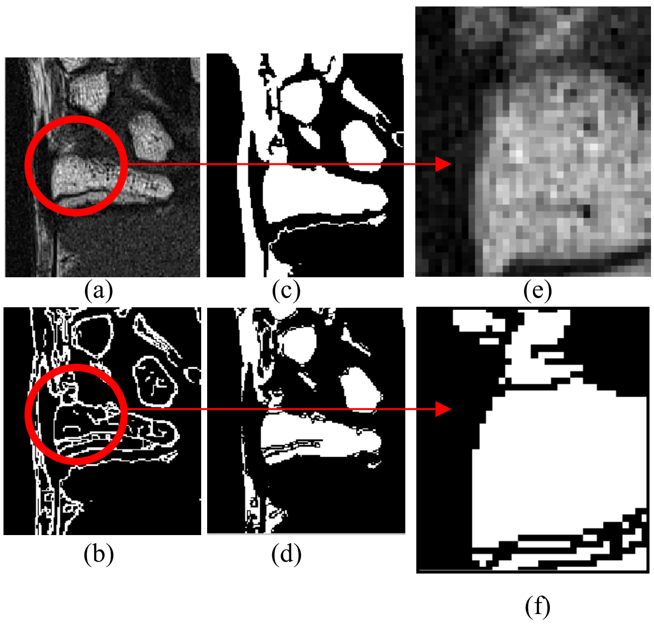

Figure 2. Approximate image of radius bone. (a) original image (b) edge map focusing example (c) the first phase outcome (d) the second phase outcome (e), (f) the magnified regions shown in (a), (b) respectively

In Fig. 2 (a) an original data is shown. The result of edge map focusing method is demonstrated in (b). We show the first and second phases' outcomes in (c) and (d) respectively. The magnified regions which we showed in (a), (b), are brought in (e), (f) respectively.

C. ROI extraction

We use the present information of the data set images o identify the initial slice. Since the radius bone has the largest region in median slices, the initial slice can be identified by searching for a slice which has the most number of pixels 1. By using morphology operator closing, we remove small area regions and consider the region with largest structure as initial mask. At the next step, we use a 3D approach, starting from the initial slice and the resulted mask, to derive the radius region for the previous and the next slices. This procedure repeats for all slices, as is brought in (3). The proposed method extracts the radius bone automatically and does not need to interaction with the user or use of seed point.

$$\begin{cases} RB^i = select(S^i \times Mask^{i+1}) \ \ for \ \ 1 \le i \le initial\,slice - 1 \\ RB^{initial} = Mask^{initial} \qquad i = initail\,slice \\ RB^i = select(S^i \times Mask^{i-1}) \ \ for \ \ initial\,mask + 1 \le i \le 27 \end{cases} \tag{3}$$

In (3), RB^i is the approximated segmented radius bone in i-th slice and S^i is the binary image of output of (2) which multiplied by $Mask^i$.

As we said, the extraction of radius by edge map focusing method is a non-exact estimation of radius bone. But, it can be used as an initial value or ROI in dynamic segmentation algorithms. So, the convex hull is applied to (3) and the outcome is considered as ROI. In the next section we elaborate the exact segmentation algorithm by using active contour.

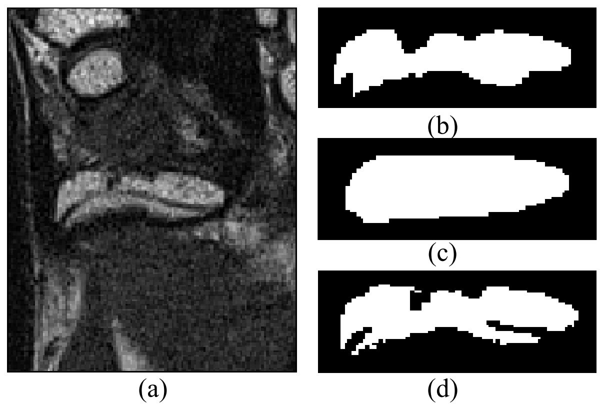

Figure 3. An example of region of interest extraction: (a) original image (b) approximate image of radius bone (c) convex hull of the approximate image as ROI (d) the output segmented by active contour.

D. Segmentation based on active contour

For a good segmentation of the bone structures in the MRI 3D datasets, an appropriate initialization is required. It does not have to be very accurate, but it has to provide starting contours (or volumes for the 3D case) for each bone to be segmented (see Fig. 4).

Active contour methods can intuitively be understood as digitally-generated curves operating within images with the aim of identifying object boundaries. Initially named snakes [8], they are energy minimizing splines, moulding a closed contour to image object boundaries by means of deformation under the influence of image forces, internal forces and external constraint forces [8]. Considering that the snake (contour) position at time t can be parametrically represented by $\upsilon(s,t)=[x(s,t)\ y(s,t)]$, the evolution of the deformable model can be represented as shown in (4), where $\mu(s)$ and $\gamma(s)$ control the mass and the damping density of the contour. The model is moving under the influence (magnitude and direction) of the internal and external forces.

$$\mu(s)\frac{\delta^2\upsilon(s,t)}{\delta t^2}+\gamma(s)\frac{\delta\upsilon(s,t)}{\delta t}=F_{\text{int}}+F_{ext} \quad (4)$$

The most commonly used formulation for the internal energies is shown in (5), where $\alpha(s)$ and $\beta(s)$ manage the tension and the exibility of the contour. The external potentials are defined based on the gradients or other features in the image [8].

$$F_{\text{int}}=\frac{1}{2}(\alpha(s)\left|\frac{\delta\upsilon(s,t)}{\delta s}\right|^2+\beta(s)\left|\frac{\delta^2\upsilon(s,t)}{\delta s^2}\right|^2) \quad (5)$$

Some of the disadvantages of this approach are the sensitivity of the snake evolution to the initialization and poor convergence in concave regions [9].

The proposed segmentation algorithm based on active contour in comparison to other methods such as level set, is easy and has less computational complexity. It also, because of using a proper initial value, is less time consuming.

Unlike to other segmentation algorithms, such as region growing, which need to manual initial value or seed points, the proposed algorithm is fully automatic and does not have the problem of convergence.

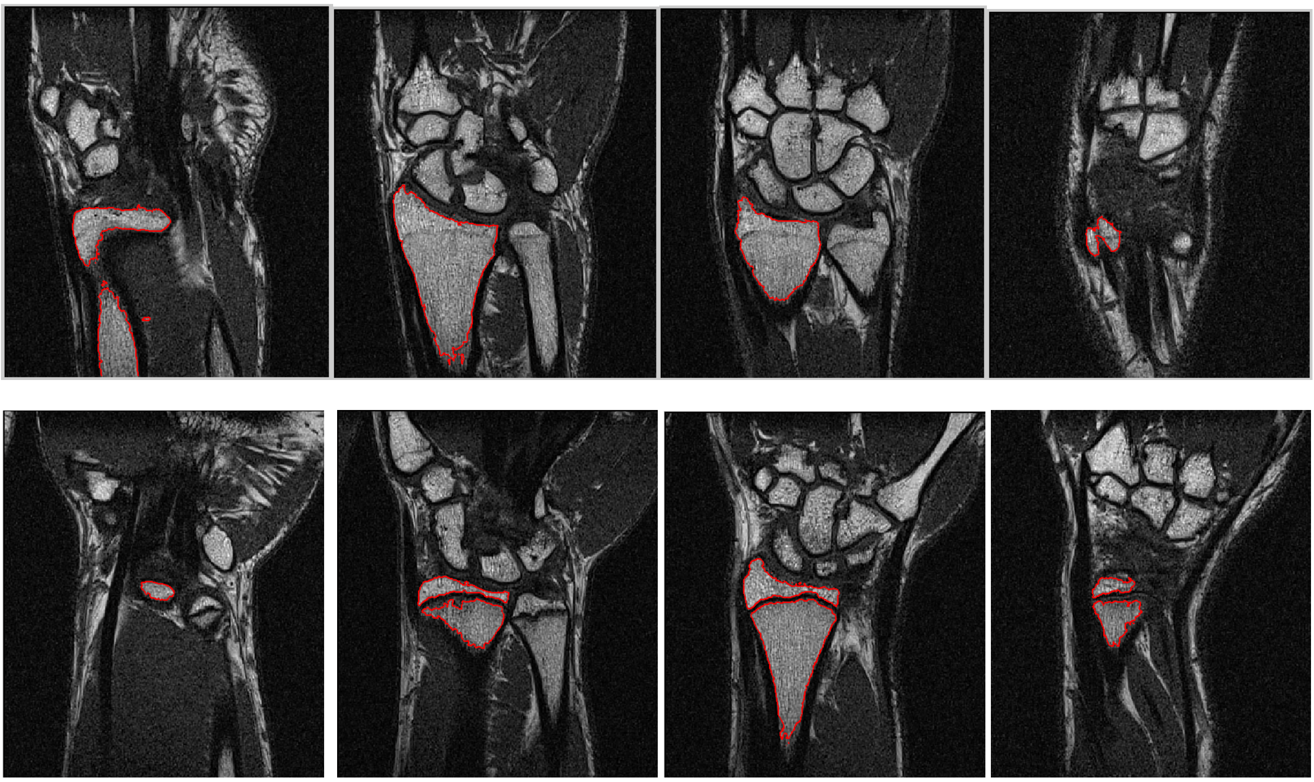

(a) (b) (c) (d)

Figure 4. Final active contour segmentation from coronal slices for a subject with closed Epiphyseal plate (top) and another subject with open Epiphyseal plate (bottom): (a), (b), (c), (d): 6, 12, 18, 24-th slices respectively.

III. Results

The proposed method is applied to 23 subjects' images, for each subject 27 slices, data set. We observe an error in segmentation outcomes in 8 slices among more than 600 slices. So, the accuracy of the algorithm is % 98.67. We compared the outcomes of the automatic segmentation with the manual segmentation under specialized physician's supervision. (see Fig. 5)

The main goal of the segmentation algorithms is to capture as accurate as possible the structures of interest. For the assessment of their performances, the segmentation results are compared with manually segmented ground truth using several quality measures.

The true positive rate, also called sensitivity, measures the rate of the accurately recognized positives (6). On the other hand, specificity quantifies the capability of correctly detecting negatives (8).

Accuracy is related to the rate of correct results with respect to the whole domain (7) and precision is the percentage of the accurately identified positives with respect to all positive results (9). As well, in the case of these measures, higher percentages refer to higher performances of the assessed segmentation algorithm.

The similarity between the ground truth and the segmentation results can be also computed using the Dice coefficient and is defined as shown in (10). A low value for the Dice coefficient would suggest that there is low similarity between the ground truth and the outcome of the segmentation algorithm, while a unity coefficient would denote a perfect segmentation.

$$sensitivity = \frac{TP}{TP + FN} \tag{6}$$

$$accuracy = \frac{TP + TN}{TP + FP + FN + TN} \tag{7}$$

$$specificity = \frac{TN}{FP + TN} \tag{8}$$

$$precision = \frac{TP}{TP + FP} \tag{9}$$

$$Dice\,coefficient = \frac{2TP}{(TP + FP) + (TP + FN)} \tag{10}$$

We also compared the proposed fully automatic algorithm with the manual algorithm in terms of kappa criteria. For kappa statistic, each voxel is observed by both target and source volume. Each volume gives a label to each voxel [10].

According to Table 1, the results show that the proposed method outperforms the manual segmentation method in term of quality measures which we brought in the table.

Figure 5. Comparison of the proposed method output vs. the manual segmentation. White pixels are TP, pink pixels are FP, green pixels are FN, and the rest pixels are TN. (a), (b), (c): three different subjects.

Table 1. Quality measures for the 3D bone segmentation

Quality measures	Sensitivity	Accuracy	Specificity	Precision	**Dice**	**Kappa Statistics**
active contour segmentation	0.9008	0.9987	0.9992	0.9653	**0.9482**	**0.9246**
edge map focusing segmentation	0.8213	0.9927	0.9813	0.8631	0.8542	0.8084

IV. Conclusion

In this paper we proposed a fully automatic algorithm for segmentation of radius bone based on active contour method. The implemented segmentation algorithm comprises several stages for the successful accomplishment of the task. The first step takes into account the pre-processing of the images to be analysed for reducing the noise and enhancing the features of interest for the subsequent segmentation algorithms. the next section discusses initialization techniques. Finally, active contour methods are introduced, as they are one of the most used techniques in medical image segmentation. We applied the algorithm to the MR images of 23 subjects' hand wrists. Our method does not need to a human intervention or seed points. The bone segmented image can be used in finding the epiphyseal plate in order to define the subject's bone age.

Acknowledgment

We appreciate the radiology authorities of Payambaran hospital who provided us with the data we used in this study.

REFERENCES

[1] M. Droske, B. Meyer, M. Rumpf, and C. Schaller, "An adaptive level set method for medical image segmentation," in *Information Processing in Medical Imaging*, 2001, pp. 416-422.

[2] J. Krátký and J. Kybic, "Three-dimensional segmentation of bones from CT and MRI using fast level sets," in *Proc. of SPIE Vol*, 2008, pp. 691447-1.

[3] A. A. Farag, H. Hassan, R. Falk, and S. G. Hushek, "3D volume segmentation of MRA data sets using level sets: image processing and display," *Academic radiology,* vol. 11, pp. 419-435, 2004.

[4] A. Bosnjak, G. Montilla, R. Villegas, and I. Jara, "3D segmentation with an application of level set-method using MRI volumes for image guided surgery," in *Engineering in Medicine and Biology Society, 2007. EMBS 2007. 29th Annual International Conference of the IEEE*, 2007, pp. 5263-5266.

[5] V. Caselles, R. Kimmel, and G. Sapiro, "Geodesic active contours," *International journal of computer vision,* vol. 22, pp. 61-79, 1997.

[6] C. Li, R. Huang, Z. Ding, C. Gatenby, D. Metaxas, and J. Gore, "A variational level set approach to segmentation and bias correction of images with intensity inhomogeneity," in *Medical Image Computing and Computer-Assisted Intervention–MICCAI 2008*, ed: Springer, 2008, pp. 1083-1091.

[7] R. D. Nowak, "Wavelet-based Rician noise removal for magnetic resonance imaging," *Image Processing, IEEE Transactions on,* vol. 8, pp. 1408-1419, 1999.

[8] M. Kass, A. Witkin, and D. Terzopoulos, "Snakes: Active contour models," *International journal of computer vision,* vol. 1, pp. 321-331, 1988.

[9] T. F. Chan and L. A. Vese, "Active contours without edges," *Image Processing, IEEE Transactions on,* vol. 10, pp. 266-277, 2001.

[10] A. F. Frangi, D. Rueckert, J. A. Schnabel, and W. J. Niessen, "Automatic construction of multiple-object three-dimensional statistical shape models: Application to cardiac modeling," *Medical Imaging, IEEE Transactions on,* vol. 21, pp. 1151-1166, 2002.

978-1-4799-3232-0/13/$31.00 ©2013 IEEE